ORIGINAL PAPER

Effect of modified carrier fluoride on the performance of Ni–Mo/Al$_2$O$_3$ catalyst for thioetherification

Zhao Han[1,2] · Zhuang Ma[1] · Cheng-Bo Wang[1] · Chun-Yu He[1] · Ming Ke[1] · Qing-Zhe Jiang[1] · Zhao-Zheng Song[1]

Abstract

An alumina support was modified by fluorine via impregnation to investigate the effect of fluoride content on the reactivity of Ni–Mo/Al$_2$O$_3$ catalyst. The catalyst was characterized by X-ray diffraction, N$_2$ adsorption–desorption (Brunauer–Emmett–Teller) isotherms, temperature-programmed desorption of ammonia, X-ray photoelectron spectroscopy and high-resolution transmission electron microscopy. Sulfur etherification performance of the catalyst was studied using a fixed-bed reactor. The results show that increasing fluoride content increases the pore volume and pore size but reduces the specific surface area. In addition, the degree of sulfidation of Ni first increases and then decreases. The amounts of strong acid and total acid also increase with increasing fluoride content. Performance evaluation of the catalyst reveals that the fluoride content has a minor effect on the thioetherification performance of the catalyst; however, an optimum fluoride content, which was determined to be 0.2%, can ensure lower olefin saturation and an efficient diene selective hydrogenation.

Keywords Fluorine · Thioetherification · Fluorinated ammonia · Selective hydrogenation · NiMo/γ–Al$_2$O$_3$

1 Introduction

Automobile exhaust emissions are largely accountable for haze. One of the important measures to control automobile exhaust emissions is to improve the quality of automobile gasoline. Fluid catalytic cracking (FCC) gasoline, characterized by high sulfur and olefin contents, is the main blending component of automotive gasoline in China. Therefore, the key to achieve cleaner gasoline in China is to reduce the sulfur and olefin contents of FCC gasoline and to minimize its octane loss to the highest possible extent. At present, a clean production of catalytic gasoline is realized worldwide by the selective hydrodesulfurization technology (Huang et al. 2018a, b; Yu et al. 2016; Zhang et al. 2018), in which

the thioetherification and diolefin selective hydrogenation (Miller et al. 2000; Toba et al. 2005) are the key processes.

The full-fraction FCC gasoline converts small molecules of mercaptans into larger thioethers through thioetherification. The light fractions with ultra-low sulfur and high olefin contents, together with heavy fractions of high sulfur contents, were separated by rectification. Following this, the heavy fractions were directed into the selective hydrodesulfurization device for deep desulfurization, during which the diolefin in the gasoline was also selectively hydrogenated in the thioetherification reaction. This prevented the influence of the diene on the downstream selective hydrodesulfurization catalyst, thereby maintaining its activity and stability (Frey 1998; Hearn 1996; Hearn et al. 2002). This process removes mercaptan sulfur from gasoline by sulfide etherification and prevents the saturation of light olefin-rich components in the entire selective hydrodesulfurization process, resulting in large loss of octane number of gasoline (Nocca and Debuisschert 2002; Rock and Shorey 2003). Another outstanding advantage of using thioetherification to desulfurize mercaptan is that no alkali is needed in this process. This avoids any problems related to disposal of waste alkali residues, thereby rendering this process more environmentally friendly.

Edited by Xiu-Qiu Peng

Zhao Han and Zhuang Ma have contributed equally to this work

✉ Zhao-Zheng Song
song@cup.edu.cn

1 College of Science, China University of Petroleum, Beijing 102249, China

2 PetroChina Beijing Marketing Company, Beijing 100101, China

Nowadays, thioetherification catalysts mainly load NiO and MoO$_3$ on alumina supports. Modification of the catalysts has become an important strategy to further improve the catalytic activity, selectivity and service life of the catalysts (Hartwig 2008; Huang et al. 2018a, b; Liu and Szostak 2018; Rodriguez et al. 1999; Shen et al. 2015). Among the numerous modification strategies, synthesis of fluorine-modified γ-Al$_2$O$_3$ was one of the most effective (Flego and Parker Jr 1999; Kwak et al. 2000; Lewis et al. 1989). A previous study (Rodriguez et al. 1999) has shown that the introduction of F in a catalyst support can change the acid content and acid distribution of the catalyst and is conducive to the dispersion and existence of metals in the catalyst support, as well as to the specific surface and pore structure of the support. F is highly electronegative, and hence, when Ni and Mo are loaded on the catalyst, electrons on the surface of adjacent metal atoms are attracted toward it, leaving the metals in an electron-deficient state. These are available for the formation of metal sulfide during the vulcanization of the metals. In this study, the effect of carrier fluoride modification on the activity of thioetherification catalyst was investigated, together with the selectivity of the catalyst after the introduction of F.

2 Experiment

2.1 Preparation of catalyst

An appropriate amount of dilute nitric acid solution was added to the homogeneous mixture of pseudo-boehmite and sesbania powder and extruded by twin-screw extruder. Following this, it was dried in an oven at 110 °C for 8 h, placed in a muffle furnace at 550 °C for 4 h, ground and sieved. A 20–40-mesh sieve was selected to obtain the Al$_2$O$_3$ carrier. The carrier was impregnated with different mass fractions of NH$_4$F solution, such that the loading of F on the carrier was 0.2%, 0.4%, 0.6%, 0.8% and 1.0% of the total mass of the carrier. After this, the fluorine-modified Al$_2$O$_3$ carrier was impregnated simultaneously with aqueous solutions of ammonium molybdate and nickel nitrate; the MoO$_3$ and NiO contents in the obtained sample were equal. After each impregnation step, the samples were first dried naturally, then dried at 110 °C for 8 h and then roasted at 550 °C for 4 h. Correspondingly, the samples were named F-1, F-2, F-3, F-4 and F-5. The untreated catalyst (without ammonia fluoride solution treatment) was used as blank sample and will be referred to as C-1.

2.2 Characterization of catalyst

X-ray diffraction (XRD): XRD-ray diffractometer (Bruker D8 Advance, Germany) was used for the phase analysis and characterization of the samples. The X-ray source was Cu Kα, tube voltage was 40 kV, tube current was 30 mA, scanning rate was 4° min^{-1}, and scanning range was 5°–90°. The data were collected automatically by a computer.

N$_2$ adsorption–desorption (BET) isotherm: The BET isotherm was recorded on an ASAP 2020 automatic specific surface area and pore diameter distribution instrument from Micromeritics, USA. The adsorbed gas was a mixture of nitrogen and helium, in which nitrogen and helium were the adsorbed gas and carrier gas, respectively. The adsorption measurement was carried out at 77 K. The specific surface area was calculated by the multi-point BET method. The pore size was 0.35–500 nm, resolution of microporous region was 0.1 nm, and the minimum detection value of pore volume was 0.0001 cm^3 g^{-1}.

Temperature-programmed desorption of ammonia (NH$_3$-TPD): The automatic chemical adsorbent of Autochem II 2920 made in the USA was used. The sample quantity was 0.2 g, particle size was 20–40 mesh, and pretreatment was carried out at 500 °C for 30 min. Ar was the carrier gas at a flow rate was 40 mL min^{-1}. Ammonia flow rate was 20 mL min^{-1}; adsorption was measured at 100 °C for 30 min and temperature programmed at 10 °C min^{-1} up to 800 °C. The outputs were simultaneously detected by thermal conductivity cell detector and mass spectrometry detector.

X-ray photoelectron spectroscopy (XPS): The Mo and Ni species on the surface of the sulfided catalyst were analyzed by K-α X-ray photoelectron spectrometer (Thermo Fisher). Using Al Kα X-ray as excitation source, a base vacuum of 3×10^{-9} mbar was attained, and the spectra were corrected by electron binding with C 1 s peak (284.8 eV) of the contaminated carbon. XPS analysis of Mo and Ni 3d was carried out in order to obtain the degree of sulfidation of the active metal of the catalyst.

High-resolution transmission electron microscopy (HRTEM): Tecnai G2 F20 (FEI, USA) high-resolution transmission electron microscope was used to observe the morphology (stripe length, number of layers and other parameters) of the active components on the catalyst surface.

2.3 Evaluation of sulfide properties

Thioetherification performance was evaluated on a self-assembled micro-fixed-bed reactor. The inner diameter of stainless steel reactor tube was 10 mm, and the length was 550 mm. The reactor adopts three-stage temperature control mode. The middle constant temperature section was filled with 5 mL catalyst, and the rest were partly filled with quartz sand. The raw material is simulated FCC gasoline, which is composed of n-hexene, isoprene and n-hexane at mass fractions of 30%, 1% and 69%, respectively. Following this, 200 µg g^{-1} n-butyl mercaptan was added to the simulated oil.

Catalyst pre-sulfurization: H_2 and sulfide oil were introduced into the reaction system. The sulfide oil was petroleum ether containing 2 wt% CS_2 (90–120 °C). The pre-vulcanization conditions of the temperature-programmed pre-vulcanization process were as follows: pressure: 3 MPa, H_2/oil volume ratio: 300:1, space velocity (weight hourly space velocity): 2 h^{-1}. Vulcanization was conducted at 310 °C for 6 h. The reaction conditions were as follows: reaction pressure: 3.0 MPa, H_2/oil volume ratio: 6:1, liquid hourly space velocity: 4 h^{-1}, reaction temperature: 110 °C.

2.4 Sample analysis and data processing

The mercaptan content was determined by GB/T1792-88 potentiometric titration.

The compositions of FCC simulated oil before and after the reaction were quantitatively analyzed by SP-3420A gas chromatograph. The chromatographic data were recorded and processed by BF-2002 (Beijing Beifen-Ruili Analytical Instrument Group, China) chromatographic workstation.

The conversion formula of thiol conversion rate (X_L), selective hydrogenation rate of diolefin (X_E), olefin double-bond isomerization ratio (X_Y) and olefin saturation ratio (X_B) in the reaction process are as follows:

$$X_L = \left(1 - \frac{W_{L1}}{W_L}\right) \times 100\% \tag{1}$$

$$X_E = \left(1 - \frac{W_{E1}}{W_E}\right) \times 100\% \tag{2}$$

$$X_Y = \frac{W_{Y1}}{W_Y} \times 100\% \tag{3}$$

$$X_S = \frac{W_{S1}}{W_Y} \times 100\% \tag{4}$$

$$X_B = \left(1 - X_Y - X_S\right) \times 100\%. \tag{5}$$

In the above equations, W_L and W_{L1} represent the mass fraction of mercaptan in the sample before and after the reaction; W_E and W_{E1} represent the mass fraction of the diene in the sample before and after the reaction; W_Y and W_{Y1} are, respectively, the mass fraction of n-hexene in the raw material before the reaction and mass fraction of isomeric olefin after reaction; W_{S1} is the mass fraction of n-hexene in the sample after the reaction.

3 Results and discussion

3.1 Catalyst characterization

3.1.1 XRD analysis

The series of fluoride-modified catalysts were characterized by XRD, and the results are shown in Fig. 1. It can be seen from Fig. 1a that the characteristic peaks of γ-Al_2O_3 at 39.5°, 45.9° and 66.9° correspond to the (311) (400) and (440) crystal planes (JCPDS-0425) (Li and Shao 2008). At the same time, it is found that with increasing fluoride content, the obvious characteristic peaks of NiO crystals appearing in the spectrum at 2θ values of 37.3°, 43.4°, 63.0° and 75.6° correspond to the (111), (200), (220) and (311) crystal faces,
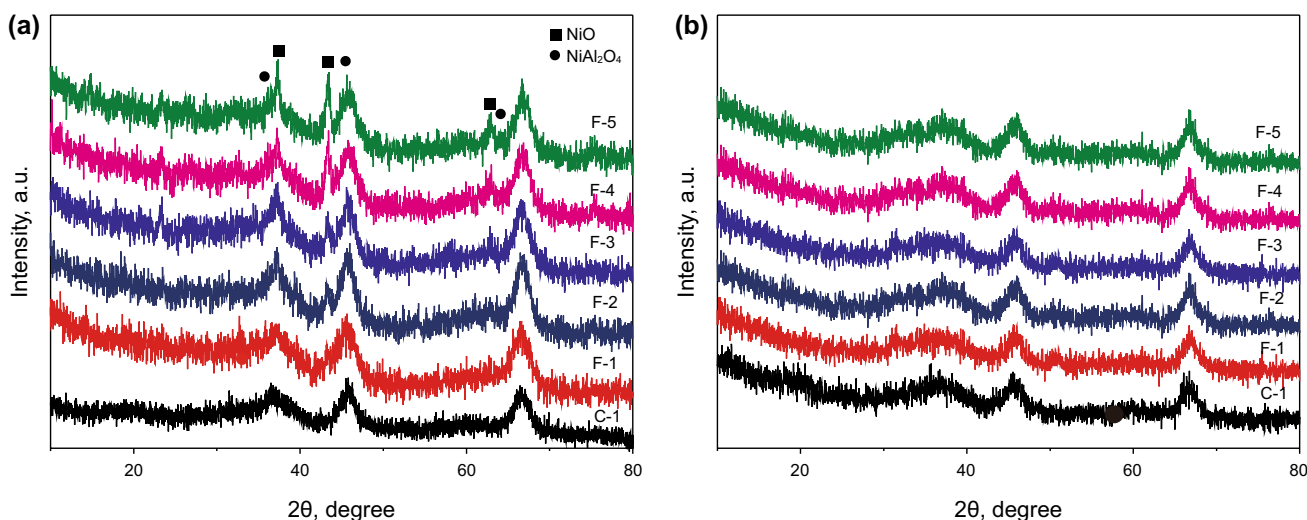

Fig. 1 XRD patterns of F–X series of catalysts: oxidized state (**a**) and sulfurized state (**b**)

respectively, of NiO crystals. In addition, analysis of the spectrum of F-5 catalyst with JADE 5.0 software reveals that the peaks of $NiAl_2O_4$ crystal appear at 27.02°, 44.98° and 65.55°, which indicates that with increasing fluoride content in the catalyst, the interaction between Ni and the carrier changes. This is detrimental to the dispersion of Ni on the catalyst. The aggregation of Ni causes the catalyst to adopt a spinel structure on the surface during firing, and this is not only harmful to the sulfuration of Ni, but can also reduce the dispersion of the active center of the catalyst, thereby affecting the activity of the catalyst.

Figure 1b shows the XRD spectra of the sulfide state of the catalyst. Compared with the oxidized state spectrum, the main characteristic diffraction peaks are the peaks of Al_2O_3 carrier. Analysis by JADE 5.0 software reveals that there are no characteristic peaks of sulfide loaded with metal, and the spinel structure disappears after sulfidation, indicating that the metal on the surface of the carrier was uniformly dispersed after the catalyst was vulcanized, and no crystal aggregation occurred.

Table 1 Textural properties of the F–X series of catalysts

Sample	Specific surface area, $m^2\,g^{-1}$	Average pore diameter, nm	Pore volume, $cm^3\,g^{-1}$
C-1	223.57	8.31	0.46
F-1	220.34	8.92	0.53
F-2	209.48	9.14	0.56
F-3	201.17	9.32	0.61
F-4	196.86	9.56	0.64
F-5	190.45	9.73	0.69

3.1.2 BET characterization

BET isotherms of the fluoride-modified catalysts were recorded, and the results are listed in Table 1.

Table 1 shows that the specific surface area of the catalysts decreases with increasing fluoride content, while the pore size and pore volume tend to increase. This may be because of the erosion of fluoride to the thin-walled structure between the channels, resulting in reduced specific surface area (Ebrahimynejad et al. 2014). In addition, the catalyst produced a large amount of AlF_3 after modification; AlF_3 has a smaller specific surface area (Benítez et al. 1996) than γ-Al_2O_3.

3.1.3 NH3-TPD characterization

NH_3-TPD characterization was carried out for the fluoride-modified catalysts, and the results are shown in Fig. 2.

Figure 2 shows the NH_3-TPD spectrum of the sulfided state of the C-1 and F–X series of catalysts. In Fig. 2a, peaks in the range 20–200 °C, 200–350 °C and 350–550 °C correspond to weak, medium and strong acidic sites interacting with NH_3 molecules (Andonova et al. 2007). As the fluoride content in the catalyst increases, the number of weak acidic sites first increases slightly and then decreases, while the amounts of strong acid and total acid increase as a function of the fluoride content. Figure 2b shows the NH_3-TPD spectrum of the F-1 catalyst before and 60 h after the reaction. As is apparent from the figure, the strong acid center in the catalyst disappears after the reaction, indicating that the strong acid center is masked during the reaction. At the same time, analysis of the peak area of the weak acid
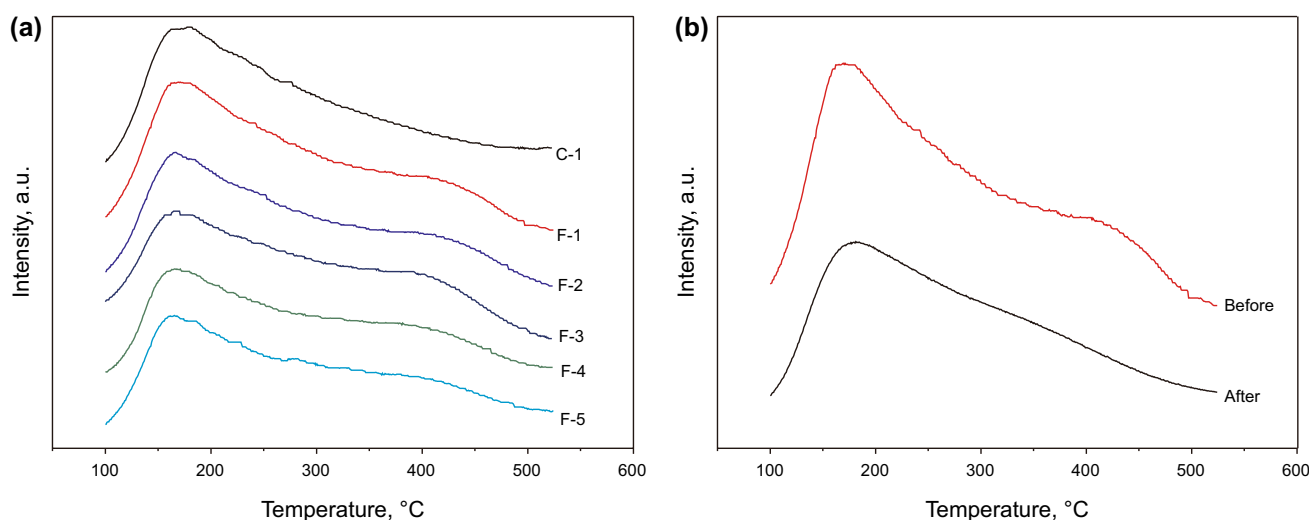
Fig. 2 NH_3-TPD patterns of sulfided F–X series of catalysts: Pre-reaction spectra of sulfide catalysts (**a**) and comparison of F-1 catalyst before and after the reaction (**b**)

peak at 180 °C suggests that the weak acidity of the catalyst decreases significantly after the reaction; the total amount of acid also decreases significantly. This can be attributed to the fact that the interaction between fluoride and the exposed OH reduces the bond energy of OH, thereby increasing the acidity of the latter (Corma et al., 1985). Lewis acid sites exist on the surface of γ-Al_2O_3, and fluoride may replace oxygen atoms or OH bonds. At low fluoride contents, the F atom may replace the OH bond on the surface of γ-Al_2O_3 and exist in the form of $AlF_i(OH)^{3-}$ ($i = 1-3$) and free radicals. With increasing fluoride content, a large amount of AlF_3 will be generated (Miciukiewicz et al. 1989; Qu et al. 1998). However, the excess acid and acid strength of the catalyst will lead to the superposition reaction of olefins on the acid sites during the reaction. Excessive superposition reaction will affect the quality of oil and reduce the octane number of oil products. Excess acidity of the catalyst will lead to the formation of carbon deposits, and the pore channels of the catalysts would be blocked. This will accelerate the deactivation of the catalysts, which is not conducive to the sulfide etherification reaction.

3.1.4 XPS characterization

The series of fluoride-modified catalysts were characterized by XPS. Figure 3 shows the XPS spectra of Ni $2p_{3/2}$ and Mo $3d$ in the vulcanized state.

Ni $2p_{3/2}$ spectrum was analyzed by means of XPS peak differentiation fitting analysis using XPSPEAK software (Fig. 3a). For the sulfided state of the three types of catalysts with a single load of Ni, the binding energies of the two species were 852.9, 856.7 and 858 eV. In analogy with the analysis by Lai et al. (Lai et al. 2013), it is estimated that the first peak corresponds to sulfided Ni species (NiS), and the latter two peaks correspond to two types of unvulcanized, oxidized Ni–Al spinel species.

The high electronegativity of F results in the attraction of electrons in the outer layer of the Ni, thereby decreasing the electron density in the outermost layer of Ni and increasing the binding energy (as seen in Fig. 3 and Table 2). For F-1, F-2 and F-3 catalysts, the degree of sulfidation of Ni increased, and the Ni_3S_2 content in F-3 catalyst reached 35.7%, which was 8.8% higher than that of unmodified C-1 catalyst. When the fluoride content in the catalyst carrier was further increased, the Ni_3S_2 content decreased. According
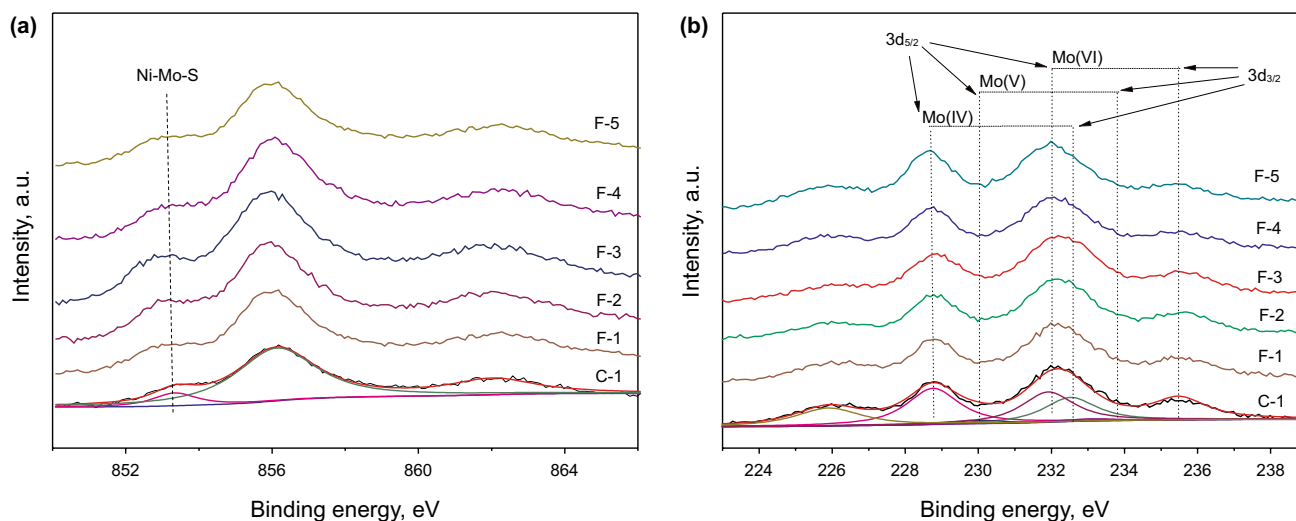

Fig. 3 Ni XPS spectrum of the F–X series of catalysts Ni $2p_{3/2}$ (**a**) and Mo $3d$ (**b**)

Table 2 Binding energy and degree of sulfidation of Ni species on the catalyst surface

Sample	Ni $2p_{3/2}$, eV	Ni_3S_2, %	Ni $2p_{3/2}$, eV	$NiAl_2O_4$, %	Ni $2p_{3/2}$, eV	$NiAl_xO_y$, %
C-1	853.7	32.8	856.4	59.3	858.0	7.9
F-1	853.8	34.3	856.4	57.1	858.1	8.6
F-2	853.9	35.7	856.5	56.2	858.2	8.1
F-3	853.9	37.6	856.7	54.8	858.2	7.6
F-4	854.1	35.1	856.7	55.9	858.4	9.0
F-5	854.3	31.2	856.6	59.5	858.5	9.3

to the BET analysis, when the fluoride content is very high, the specific surface area of the catalyst will decrease, and the aggregation of Ni will cause the catalyst to form a spinel structure on the surface during calcination. This is not conducive to the vulcanization of Ni and reduces the Ni_3S_2 content in the vulcanized catalyst.

Figure 3b shows the XPS spectra of Mo 3d of the catalyst. Based on previous studies (Ding et al., 2009; Wang and Ozkan, 2005), the sulfided Mo 3d XPS peak differentiation fitting reveals that there are S 2 s peaks (226.3 eV) (Andonova et al., 2007) and three groups of Mo $3d_{5/2}$ and Mo $3d_{3/2}$ double peaks in the series of catalysts: The first group of double peaks appears at 229.1 eV (Mo $3d_{5/2}$) and 231.8 eV (Mo $3d_{3/2}$) and corresponds to Mo (IV), i.e., completely sulfided Mo 3d species. The second group of double peaks emerging at 230.1 eV (Mo $3d_{5/2}$) and 233.5 eV (Mo $3d_{3/2}$) could be assigned to Mo(V), i.e., molybdenum oxysulfide copolymer that has not been completely vulcanized (MoO_xS_y) (Ninh et al., 2011). The third group of double peaks at 231.2 eV (Mo $3d_{5/2}$) and 235.6 eV (Mo $3d_{3/2}$) can be ascribed to Mo (VI), i.e., oxidized Mo species that are not sulfided. Table 3 shows that the binding energies of Mo (IV) $3d_{5/2}$ and Mo (IV) $3d_{3/2}$ increase slightly after fluoride modification. Compared with the C-1 catalyst, the binding energies of Mo (IV) $3d_{5/2}$ and Mo (IV) $3d_{3/2}$ of the F-5 catalyst increased by about 0.2 eV. At the same time, with increasing fluoride content in the catalyst, the degree of vulcanization of Mo increased. The degrees of sulfidation of Mo in the C-1 and F-5 catalysts are 58.3% and 64.2%, respectively, suggesting a 10% increase in the degree of sulfidation of Mo in the two catalysts.

3.1.5 HRTEM characterization

The sulfurized F–X series of catalysts were characterized by HRTEM.

Figure 4 shows the HRTEM images of the sulfided F–X catalysts. The MoS_2 structure can be clearly identified in the images. Ni could be hardly observed by HRTEM, because it is present in the corner of the MoS_2 stack. The layer number

Table 3 Binding energy and degree of sulfidation of Mo species on the catalyst surface

Sample	Mo (IV) $3d_{5/2}$, eV	Mo (IV) $3d_{3/2}$, eV	Sulfidity of Mo, %
C-1	230.1	233.4	58.3
F-1	230.18	233.43	58.9
F-2	230.24	233.48	59.4
F-3	230.29	233.51	61.7
F-4	230.31	233.55	62.8
F-5	230.33	233.62	64.2

and length of MoS_2 fringes increased obviously with the addition of fluoride in the catalyst, which was consistent with the increase in molybdenum sulfidation with increasing fluoride content. The textural properties of the MoS_2 fringes as obtained by statistical analysis are shown in Table 4. The average length of the MoS_2 fringes of the unmodified C-1 catalyst was 4.08 nm, which increased to 4.83 nm for the F-1 catalyst, corresponding to a 15.5% increase. Meanwhile, the average length of the MoS_2 fringes increased with increasing fluoride content. MoS_2 fringe length of the F-5 catalyst was 5.81 nm, which was 42.4% higher than that of the F-1 catalyst. Data analysis of MoS_2 fringe layers showed that the number of MoS_2 fringe layers in catalyst increased with the addition of fluoride, resulting in new 4–5 layered multilayer fringes. A previous study (Andonova et al. 2007) showed that the angular position of multilayer NiMoS had strong hydrogenation activity, and it was the active center of the catalyst. More the number of layers, higher will be the hydrogenation activity of the catalyst. The increase in stacking layers will increase the number of active sites at the corners, thus improving the olefin saturation performance and reducing the selectivity of the catalyst.

3.2 Catalyst performance evaluation

The reaction of F–X series of catalysts was conducted primarily to investigate the mercaptan etherification performance of the catalyst, selective hydrogenation performance of diolefins, olefin saturation and olefin isomerization performance of the catalyst.

It is evident from Fig. 5 that the addition of fluoride to the catalyst has a minor effect on the thioetherification performance and the mercaptan content is maintained above 96%. At the initial stage of the reaction, the catalyst is strongly acidic. However, as the reaction progresses, the carbon deposits on the catalyst are substantial; the hydrogenation activity decreases sharply, and the olefin isomerization and the selective hydrogenation performance of the diene of the catalyst also decrease. Higher the fluoride content of the catalyst, faster will be the decrease. Combined with the results of NH_3-TPD analysis (Fig. 2), the change in acidity of the catalyst before and after the reaction is very obvious. The strong acidic center of the catalyst after the reaction is basically absent, and the amount of weak acid is also decreased, thereby decreasing the total amount of acid significantly. It can be seen that if the fluoride content in the catalyst is very high, the activity of the catalyst rapidly decreases. The F-1 catalyst (low fluoride content) ensures good thioetherification and selective hydrogenation of the diolefin, lower olefin hydrogenation, improved selectivity and increased olefin isomerization capacity. Thus, the reaction performance of the F-1 catalyst is superior to that of the unmodified C-1 catalyst.
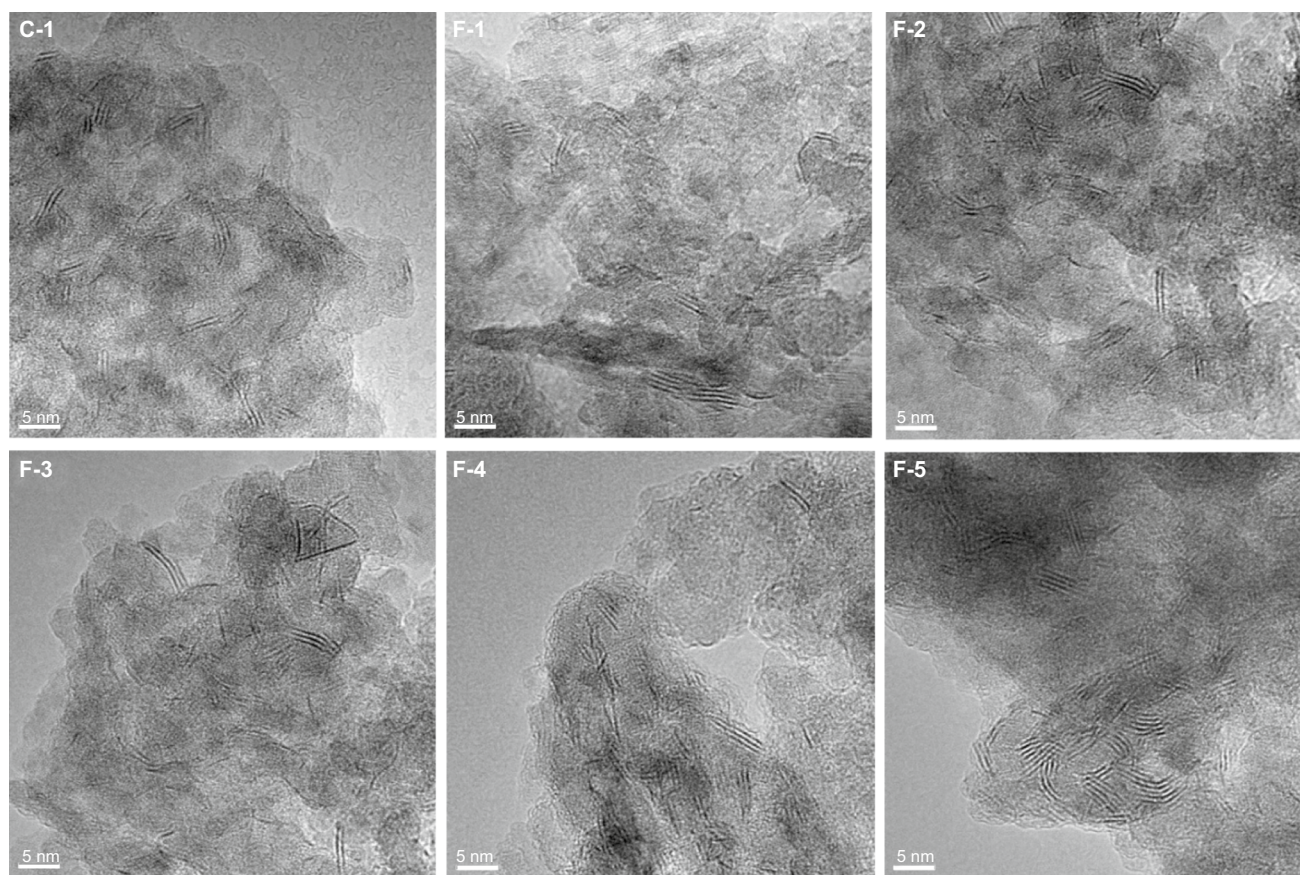
Fig. 4 HRTEM images of sulfided F–X series of catalysts

Table 4 Textural properties of MoS$_2$ on sulfided F–X series of catalysts

	C-1	F-1	F-2	F-3	F-4	F-5
Average length, nm	4.08	4.83	5.12	5.34	5.67	5.81
Main stripe number	2–3	2–4	2–4	2–4	3–4	3–5

4 Conclusion

After modification by fluoride, the pore structure changes, the catalyst has a smaller specific surface area and the pore size and pore volume increase to some extent. Simultaneously, the acidity of the catalyst is also changed. The strong acid center appeared in the fluoride-modified catalyst, and the amount of strong acid and total acid increased with increasing fluoride content. XRD shows that when the fluoride content in the catalyst is very low, the metal has a good dispersion on the surface of the support, while at high fluoride content, a distinct spinel structure appears in the catalyst.

The introduction of F changes the interaction between Ni and Mo in the catalyst and the carrier, and the degree of sulfidation of Ni is increased at low concentrations and decreased at high concentrations. The degree of vulcanization of Mo increased with increasing fluoride content. The surface morphology of the catalyst changed significantly after vulcanization. With the increase in fluoride content, the length of the stripe of MoS$_2$ increased gradually, and the number of stacking layers also increased to a certain extent. More five-layered stripes appeared in the F-5 catalyst.

The fluoride-modified catalyst showed strong hydrogenation performance at the initial stage of the reaction, but as the reaction progressed, the stronger acidic nature of the catalyst led to faster deactivation of carbon deposition. The strong acid center gradually disappeared, and the amount of acid decreased. When the reaction reaches equilibrium, the olefin hydrogenation performance and the diene selective
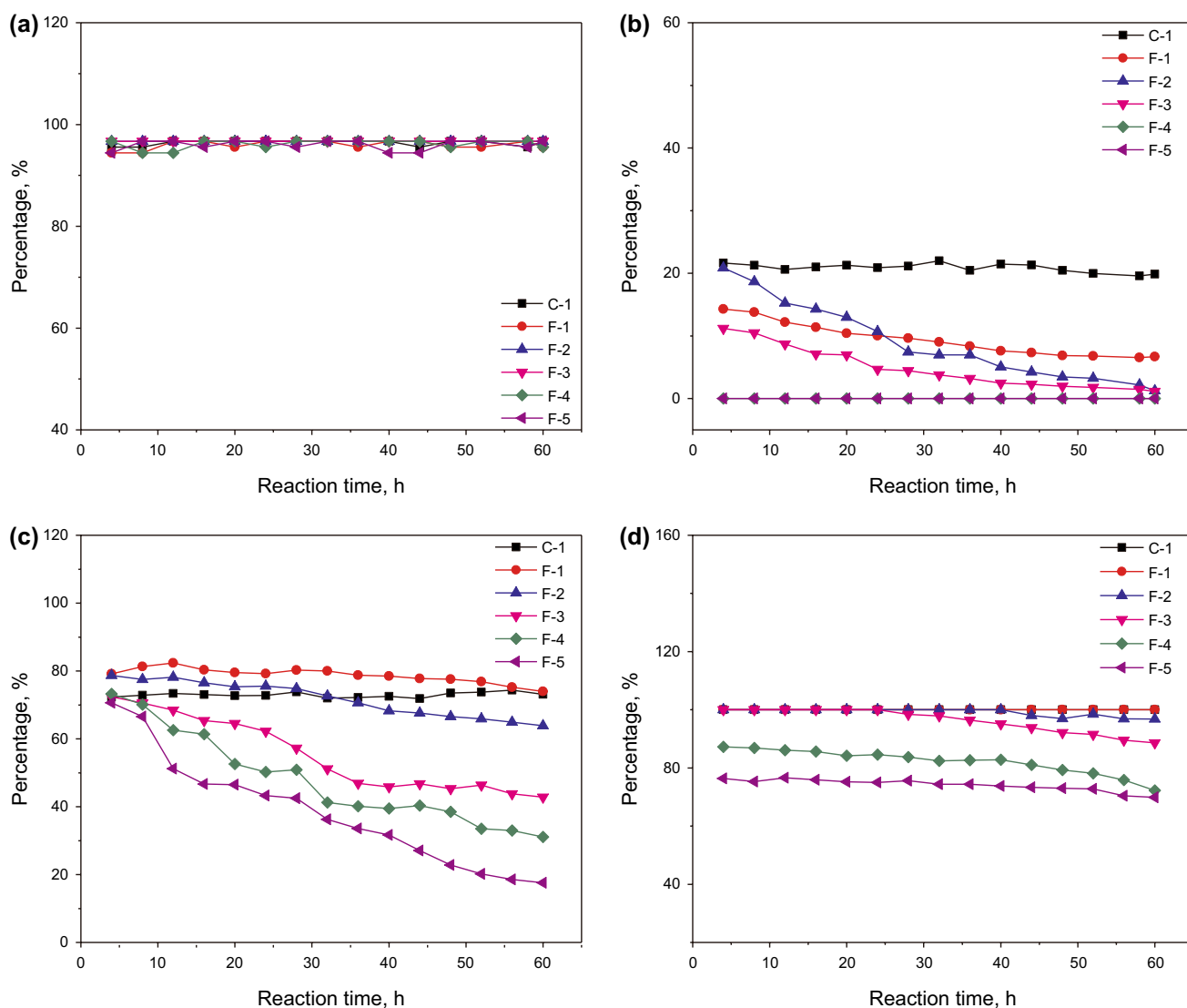
Fig. 5 Reaction performance of the F–X series of catalysts thiol conversion rate (**a**), olefin saturation rate (**b**), olefin isomerization rate (**c**) and selective hydrogenation rate of diene (**d**)

hydrogenation performance become weaker. The F-1 catalyst is a highly selective catalyst with less olefin saturation, higher selectivity and less octane number loss. It also ensures good thioetherification and selective hydrogenation performance of the diolefin.

References

Andonova S, Vladov C, Pawelec B, Shtereva I, Tyuliev G, Damyanova S, et al. Effect of the modified support γ-Al₂O₃–CaO on the structure and hydrodesulfurization activity of Mo and Ni–Mo catalysts. Appl Catal A. 2007;328:201–9. https://doi.org/10.1016/j.apcata.2007.06.009.

Benítez A, Ramírez J, Fierro JLG, Agudo AL. Effect of fluoride on the structure and activity of NiW/Al₂O₃ catalysts for HDS of

thiophene and HDN of pyridine. Appl Catal A. 1996;144:343–64. https://doi.org/10.1016/0926-860X(96)00121-4.

Corma A, Fornés V, Ortega E. The nature of acid sites on fluorinated γ-Al₂O₃. J Catal. 1985;92:284–90. https://doi.org/10.1016/0021-9517(85)90262-3.

Ding L, Ying Z, Hong Y, Parviz R. LCO hydrotreating with Mo–Ni and W–Ni supported on nano- and micro-sized zeolite beta. Appl Catal A. 2009;353:17–23. https://doi.org/10.1016/j.apcata.2008.10.023.

Ebrahimynejad M, Haghighi M, Asgari N. Ultrasound assisted synthesis and physicochemical characterizations of fluorine-modified CoMo/Al₂O₃ nanocatalysts used for hydrodesulfurization of thiophene. J Nanosci Nanotechnol. 2014;14:6848–57. https://doi.org/10.1166/jnn.2014.8966.

Flego C, Parker WON Jr. Characterization of γ-alumina and borated alumina catalysts. Appl Catal A Gen. 1999;185:137–52. https://doi.org/10.1016/S0926-860X(99)00137-4.

Frey SJ. Process for thioetherification and selective hydrogenation of light hydrocarbons. U.S. Patent No. 5,759,386. 1998.

Hartwig JF. Evolution of a Fourth Generation Catalyst for the Amination and Thioetherification of Aryl Halides. Accounts Chem Res. 2008;41:1534–44. https://doi.org/10.1021/ar800098p.

Hearn D. Process for the removal of mercaptans and hydrogen sulfide from hydrocarbon streams. U.S. Patent No. 5,510,568. 1996.

Hearn D, Gildert GR, Putman HM. Process for removal of mercaptans from hydrocarbon streams. U.S. Patent No. 6,440,299. 2002.

Huang T, Xu J, Fan Y. Effects of concentration and microstructure of active phases on the selective hydrodesulfurization performance of sulfided CoMo/Al₂O₃ catalysts. Appl Catal B. 2018a;220:42–56. https://doi.org/10.1016/j.apcatb.2017.08.029.

Huang T, Peng Q, Shi W, Xu J, Fan Y. An anionic surfactant-assisted equilibrium adsorption method to prepare highly dispersed Fe-promoted Ni/Al₂O₃ catalysts for highly selective mercaptan removal. Appl Catal B. 2018b;230:154–64. https://doi.org/10.1016/j.apcatb.2018.02.053.

Kwak C, Lee JJ, Bae JS, Choi K, Moon SH. Hydrodesulfurization of DBT, 4-MDBT, and 4, 6-DMDBT on fluorinated CoMoS/Al₂O₃ catalysts. Appl Catal A. 2000;200:233–42. https://doi.org/10.1016/S0926-860X(00)00635-9.

Lai W, Pang L, Zheng J, Li J, Wu Z, Yi X, et al. Efficient one pot synthesis of mesoporous NiMo–Al₂O₃catalysts for dibenzothiophene hydrodesulfurization. Fuel Process Technol. 2013;110:8–16. https://doi.org/10.1016/j.fuproc.2013.01.006.

Lewis JM, Kydd RA, Boorman PM. A study of fluorided Ni–Mo/Al₂O₃ catalysts in cumene conversion and thiophene HDS reactions. J Catal. 1989;120:413–20. https://doi.org/10.1016/0021-9517(89)90281-9.

Li B, Shao LL. Appraisal of alumina and aluminium hydroxide by XRD. Inorganic Chemicals Industry. 2008;2. https://doi.org/10.3969/j.issn.1006-4990.2008.02.019. **(in Chinese)**.

Liu C, Szostak M. Decarbonylative thioetherification by nickel catalysis using air- and moisture-stable nickel precatalysts. Chem Commun. 2018;54:2130–3. https://doi.org/10.1039/c8cc00271a.

Miciukiewicz J, Qader Q, Massoth FE. Studies of molybdena-alumina catalysts: XV. Effect of fluorine-modified alumina on catalyst properties. Appl Catal. 1989;49:247–57. https://doi.org/10.1016/S0166-9834(00)83021-3.

Miller JT, Reagan WJ, Kaduk JA, Marshall CL, Kropf AJ. Selective hydrodesulfurization of FCC naphtha with supported MoS₂ catalysts: the role of cobalt. J Catal. 2000;193:123–31. https://doi.org/10.1006/jcat.2000.2873.

Ninh TKT, Massin L, Laurenti D, Vrinat M. A new approach in the evaluation of the support effect for NiMo hydrodesulfurization catalysts. Appl Catal A. 2011;407:29–39. https://doi.org/10.1016/j.apcata.2011.08.019.

Nocca J, Debuisschert QP. From pilot to startup of world's first commercial 10 µg g⁻¹ FCC gasoline. Point Comfort: NPRA Annual Meeting; 2002.

Qu LL, Jian M, Shi YH, Li DD. Effect of fluorine on sulfide type NiW/γ–Al₂O₃ catalyst. Chin J Catal. 1998;19:608–9.

Rock K, Shorey S. Producing low sulfur gasoline reliably. Point Comfort: NPRA Annual Meeting; 2003.

Rodriguez LM, Alcaraz J, Hernandez M, Dufaux M, Taarit YB, Vrinat M. Fluorinated alumina: characterization of acid sites and relationship between acidity and activity in benzene alkylation. Appl Catal A. 1999;189:53–61. https://doi.org/10.1016/S0926-860X(99)00251-3.

Shen Z, Ke M, Yu P, Hu H, Song Z, Jiang Q. Reaction mechanisms of thioetherification for mercaptans and olefins over sulfided Mo–Ni/Al₂O₃ catalysts. J Mol Catal A Chem. 2015;396:120–7. https://doi.org/10.1016/j.molcata.2014.09.034.

Toba M, Miki Y, Kanda Y, Matsui T, Harada M, Yoshimura Y. Selective hydrodesulfurization of FCC gasoline over CoMo/Al₂O₃ sulfide catalyst. Catal Today. 2005;104:64–9. https://doi.org/10.1016/j.cattod.2005.03.027.

Wang X, Ozkan US. Effect of pre-treatment conditions on the performance of sulfided Ni–Mo/γ–Al₂O₃ catalysts for hydrogenation of linear aldehydes. J Mol Catal A Chem. 2005;232:101–12. https://doi.org/10.1016/j.molcata.2005.01.037.

Yu P, Ke M, Liu Q, Yan X, Li J. Enhancement of the selective hydrodesulfurization performance by adding cerium to CoMo/gamma–Al₂O₃ catalysts. RSC Adv. 2016;6:96662–8. https://doi.org/10.1039/c6ra15637a.

Zhang C, Li P, Liu X, Liu T, Jiang Z, Li C. Morphology-performance relation of (Co)MoS₂ catalysts in the hydrodesulfurization of FCC gasoline. Appl Catal A. 2018;556:20–8. https://doi.org/10.1016/j.apcata.2018.02.026.